

# Local Deformation Measurement of Biological Tissues Based on Feature Tracking of 3D MR Volumetric Images

Penglin Zhang<sup>1,2</sup>, Shinichi Hirai<sup>1</sup>, Kazumi Endo<sup>1</sup> and Shigerhiro Morikawa<sup>3</sup>

<sup>1</sup>Dept. of Robotics, Faculty of Science and Engineering, Ritsumeikan University

<sup>2</sup>School of Remote sensing and Information Engineering, Wuhan University

<sup>3</sup>Shiga University of Medical Science  
Kusatsu, Shiga 525-8577, Japan

**Abstract**—Being able to measure deformations precisely in tissue by magnetic resonance (MR) imaging is very useful for many medical imaging applications. While a variety of different algorithms have been formulated for this purpose, few are based on tracking features in the images. Here, we propose an approach of automatically extracting feature points and matching them to measure local deformation as seen in 3D MR volumetric images. Correlation scores ( $cs$ ) are given to pairs of high curvature points in a 3D cubic region to ensure that they are well matched. Those with scores above a given threshold are considered as candidate points. The strength of matching of the candidate points are evaluated using an iterative energy function, and then the well matched points are used to estimate the deformation. The approach was very effective when applied to actual MR volumetric images of a person's calf.

## I. INTRODUCTION

Pre-estimating deformation or motion of biological tissues is often required for computer-assisted medical applications, such as clinical diagnosis, surgery simulation, operation planning, and evaluation of physical characteristics of biological tissues, which are becoming increasingly more common. Images can be obtained in three dimensions (3D) using magnetic resonance (MR), computer tomography(CT), ultrasonic (US) scans, all of which are non-invasive. Magnetic resonance imaging (MRI) is particularly good for estimating deformation of tissue because it affords superb anatomic images with excellent spatial resolution and contrast between soft tissues.

Estimations of deformation from MR volumetric images are mainly based on elastic deformation models [1]-[3], which can be classified into either parametric or geometric active models [4]. In the former, parametric active contours, also called snakes, were first introduced by Kass et al. in 1987 [5], and subsequently used by Lang et al. [6], Cho et al. [2] and Matuszewski et al. [1] to estimate deformation of soft objects. Its general idea is to try to minimise the designed function to deform a given initial contour toward the boundary of the object to obtain the object's deformation. The geometric active

model was first proposed by Caselles et al. [7], and developed by Malladi et al. [8], Caselles [9] and Chenoune et al. [4]. In the geometric active model, propagation of curves and surfaces are used to detect boundaries and track motion.

Moreover, much work has also been done on MRI tagging technique for measuring deformation. The MRI tagging method was proposed by Zerhouni [11], and has been subsequently developed: Amini et al. [12] introduced a coupled B-snake grids and constrained thin-plate splines to analyze 2D tissue deformations; Wang et al. [14] proposed using subspace approximation techniques to compute motion fields and introduced a spline technique to reconstruct dense displacement fields; Chen et al.[28] introduced an approach for tracking the tags; and Huang et al.[13] introduced an environment to fit and track volumetric tagged MRI data by a 4D deformable B-spline model. In all these MRI tagging methods, a set of radio-frequency (RF) pulses are used to make trackable tags in thin slices perpendicular to the imaging plane [12].

Although the algorithms used to measure the deformations have been much improved in recent years, some problems still remain. The parametric active model cannot handle changes in the topology of the evolving contours when implementations of deformation made are performed directly, and special, often heuristic, topology handling procedures must be used [9]. In the geometric active model, when contrast is poor and boundaries are not clear or continuous in the images, the contours tend to leak through the boundary [10]. The tagged images must have a regular grid pattern in the imaging plane, and if the number of tagged points is low the accuracy of the measurements will be poor.

Herein, we propose an approach based on matching point features to measure local deformation of biological tissues from MR volumetric images. Briefly, we extract enough points of high curvature (also called points of interest) automatically in MR volumetric images taken before and after deformation of the tissue, which hereafter we refer to as initial and

deformed images, and then compare their relative positions. We describe the approach in Section 2 and give examples and preliminary experimental results in Section 3. In the final section, we present a discussion and conclusions.

## II. METHOD

Our approach consists of three steps: registration, point feature matching and deformation measurement.

### A. Registration

Registration is determination of the absolute orientation of one data set with respect to another [25]. Its application to MR images has been well studied [17]-[23]. Registration is usually applied to non-rigid objects using either a voxel-based or a feature-based method [23]. In [23], in the former method, optimized transformation is performed to maximize the difference in intensity in regions where the intensity would otherwise be similar in the initial and deformed images. The latter method uses information from different identifiable structures of the object.

In the present study, we use a registration technique to find the movement of two coordinate systems in initial and deformed MR volumetric images of a volunteer's calf (Figure 1). We select features, considered rigid, around the bone (Figure 2a) in the initial image and compare them with their corresponding features in the deformed image to obtain rotation matrix  $\mathcal{R}$  and translation vector  $\tau$ .

Denoting the position vector in the initial and deformed volumetric images as  $\mathbf{x}_i$  and  $\mathbf{x}_d$ , respectively, and consideration their geometric movement, we have affine transformation

$$\mathbf{x}_d = \mathcal{R}\mathbf{x}_i + \boldsymbol{\tau}. \quad (1)$$

$\mathcal{R}$  and  $\boldsymbol{\tau}$  can be estimated using a set of rigid features. Using the quaternion  $q_0$ ,  $q_x$ ,  $q_y$  and  $q_z$  (Horn [24]) in the rotation matrix  $\mathcal{R}$ , we can obtain equation (2) with the constraint  $q_0^2 + q_x^2 + q_y^2 + q_z^2 = 1$ .

$$\mathcal{R} = \begin{pmatrix} q_0^2 + q_x^2 - q_y^2 - q_z^2 & 2(q_x q_y - q_0 q_z) & 2(q_x q_z + q_0 q_y) \\ 2(q_y q_x + q_0 q_z) & q_0^2 - q_x^2 + q_y^2 - q_z^2 & 2(q_y q_z - q_0 q_x) \\ 2(q_z q_x - q_0 q_y) & 2(q_z q_y + q_0 q_x) & q_0^2 - q_x^2 - q_y^2 + q_z^2 \end{pmatrix} \quad (2)$$

Let  $n$  be the number of selected rigid features, and  $\mathbf{x}_{ik}$  ( $k = 1, 2, \dots, n$ ) be their position vectors in the initial volumetric image and  $\mathbf{x}_{dk}$  ( $k = 1, 2, \dots, n$ ) be their corresponding the position vectors in the deformed volumetric image. Let  $\bar{\mathbf{x}}_i$  and  $\bar{\mathbf{x}}_d$  represent their centroids in the initial and deformed images, respectively. We can write

$$\bar{\mathbf{x}}_i = \frac{1}{n} \sum_{k=1}^n \mathbf{x}_{ik}, \quad \bar{\mathbf{x}}_d = \frac{1}{n} \sum_{k=1}^n \mathbf{x}_{dk}. \quad (3)$$

To find the rotation, let us denote the new coordinates as

$$\mathbf{x}'_{ik} = \mathbf{x}_{ik} - \bar{\mathbf{x}}_i, \quad \mathbf{x}'_{dk} = \mathbf{x}_{dk} - \bar{\mathbf{x}}_d. \quad (4)$$

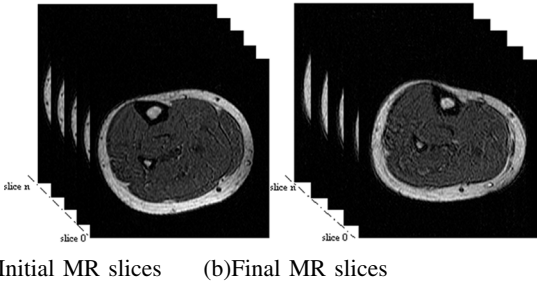


Fig. 1. Original MR volumetric image

We then introduce a  $3 \times 3$  matrix  $\mathbb{M}$  computed by the sums of cross products of coordinates measured in the initial volumetric image and those measured in the deformed volumetric image.

$$\mathbb{M} = \sum_{k=1}^n \mathbf{x}'_{ik} \mathbf{x}'_{dk}^T \quad (5)$$

According to Horn [24], the above matrix contains all the information required to solve the least-squares problem for rotation.

Note that the  $3 \times 3$  matrix  $\mathcal{A} = \mathbb{M} - \mathbb{M}^T$  is skewed symmetric, implying that multiplying matrix  $\mathcal{A}$  and a 3-dimensional vector will give the outer product of vector  $\delta$  and the vector. Letting  $\mathcal{A}_{i,j}$  be the  $(i, j)$ -th element of matrix  $\mathcal{A}$ , vector  $\delta$  is given by

$$\delta = [\mathcal{A}_{2,3} \quad \mathcal{A}_{3,1} \quad \mathcal{A}_{1,2}]^T \quad (6)$$

Let us introduce a new  $4 \times 4$  real symmetric matrix:

$$\mathcal{B} = \left( \begin{array}{c|c} \text{trace}(\mathbb{M}) & \delta^T \\ \hline \delta & \mathbb{M} + \mathbb{M}^T - \text{trace}(\mathbb{M})\mathbf{E} \end{array} \right) \quad (7)$$

where  $\text{trace}(\mathbb{M})$  is the trace of matrix  $\mathbb{M}$ , and  $\mathbf{E}$  is a  $3 \times 3$  unit matrix.

It can be shown that the unit quaternion  $\mathbf{q} = [q_0, q_x, q_y, q_z]$  is the eigenvector corresponding to the largest positive eigenvalue of matrix  $\mathcal{B}$  [24][25]. This implies that rotation matrix  $\mathcal{R}$  can be estimated. The translation vector  $\boldsymbol{\tau}$  is computed as

$$\boldsymbol{\tau} = \mathcal{R}\bar{\mathbf{x}}_i - \bar{\mathbf{x}}_d. \quad (8)$$

Figures 2b and 2c show the results of registering a 2D and a 3D image, respectively. The blue and orange contours represent the surfaces in the initial and deformed images, respectively.

### B. Point feature matching

Point feature matching is central to our approach. First, we compute a correlation score [26][27] between two cubic regions around a feature point in initial and deformed volumetric images, and then disambiguate matches through a relaxation labeling technique.

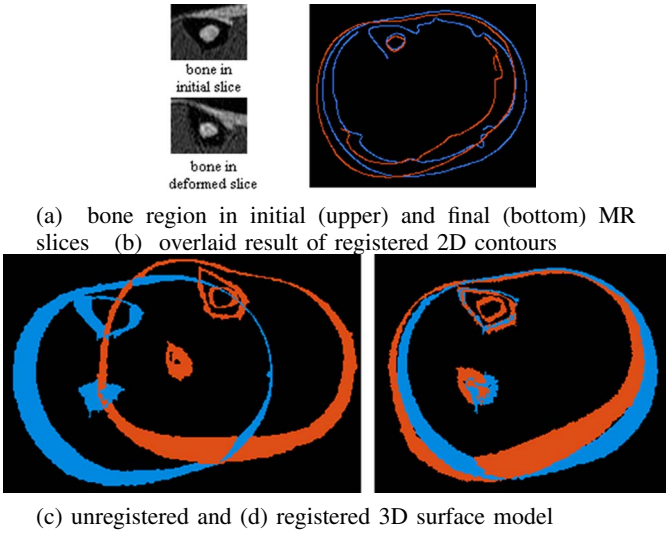


Fig. 2. Original MR volumetric image

1) *First matching through correlation score:* Given a high curvature point  $\mathbf{p}_1$  pre-extracted from the initial MR volumetric image using a Harris operator [31], we first compute its projection point  $\mathbf{p}_2$  in the deformed volumetric image using equation (1). We then select a match cubic region of size  $(2m+1) \times (2n+1) \times (2h+1)$  and search the cubic region of size  $(2u+1) \times (2v+1) \times (2w+1)$  around  $\mathbf{p}_1$  and  $\mathbf{p}_2$ . The search cube size reflects a pre-estimation of maximum deformation. The match and search cubic regions can be described as

$$\mathcal{C}_m = \{\mathbf{x} = [x \ y \ z]^T \mid x \in [-m, m], y \in [-n, n], z \in [-h, h]\}, \quad (9)$$

$$\mathcal{C}_s = \{\mathbf{x} = [x \ y \ z]^T \mid x \in [-u, u], y \in [-v, v], z \in [-w, w]\}. \quad (10)$$

Let  $g_{(\mathbf{x})}$  and  $g'_{(\mathbf{x})}$  be the voxel value of the initial and deformed volumetric images at point  $\mathbf{x}$ . The correlation score between two match cubic regions around voxel  $\mathbf{p}_1$  in the initial volumetric image and voxel  $\mathbf{p}_2$  (high curvature points within the search cube around  $\mathbf{p}_2$ ) in the deformed volumetric image is defined by

$$cs(\mathbf{p}_1, \mathbf{p}_2) = \frac{\sum_{\mathbf{x} \in \mathcal{C}_m} (g_{(\mathbf{p}_1+\mathbf{x})} - \bar{g}_{(\mathbf{p}_1)})(g'_{(\mathbf{p}_1+\mathbf{x})} - \bar{g}'_{(\mathbf{p}_2)})}{|\mathcal{C}_m| \sqrt{\sigma^2(g_{(\mathbf{p}_1)}) \times \sigma^2(g'_{(\mathbf{p}_2)})}} \quad (11)$$

where

$$|\mathcal{C}_m| = (2m+1)(2n+1)(2h+1),$$

$$\bar{g}_{\mathbf{p}_1} = \frac{1}{|\mathcal{C}_m|} \sum_{\mathbf{x} \in \mathcal{C}_m} g_{(\mathbf{p}_1+\mathbf{x})}, \quad \bar{g}'_{\mathbf{p}_2} = \frac{1}{|\mathcal{C}_m|} \sum_{\mathbf{x} \in \mathcal{C}_m} g'_{(\mathbf{p}_2+\mathbf{x})}.$$

Here,  $\sigma(g_{(\mathbf{p})})$  is the standard derivation of MR volumetric image  $g_{(\mathbf{p})}$  in the neighborhood  $(2m+1) \times (2n+1) \times (2h+1)$

of point  $\mathbf{p}$ , given by

$$\sigma^2(g_{\mathbf{p}}) = \frac{\sum_{\mathbf{x} \in \mathcal{C}_m} (g_{(\mathbf{p}+\mathbf{x})} - \bar{g}_{\mathbf{p}})^2}{|\mathcal{C}_m|} \quad (12)$$

where  $\bar{g}_{\mathbf{p}}$  is the averaged intensity in the neighborhood of point  $\mathbf{p}$  in the MR volumetric image. The correlation score ranges from  $-1$  when the cubic regions are completely different to  $1$  when they are identical.

From the correlation scores, we obtain a set of many-to-many matches, that is, a point in the initial volumetric image may be paired with more than one point (candidate matches) in the deformed image, and vice versa. Obviously, many candidate matches will be ambiguous, but this problem can be resolved with relaxation techniques [26].

2) *Definition of strength of the match:* To iteratively disambiguate the matches, we use a function for the strength of the match (SM). Let  $\mathbf{p}_{1i}$  and  $\mathbf{p}_{2j}$  represent candidate matches in initial and deformed volumetric image respectively, then,  $\mathbf{p}_{1i}$  and  $\mathbf{p}_{2j}$  can be regarded as a pair of potential matched PM( $\mathbf{p}_{1i}, \mathbf{p}_{2j}$ ) if and only if the  $SM(\mathbf{p}_{1i}, \mathbf{p}_{2j})$  between  $\mathbf{p}_{1i}$  and  $\mathbf{p}_{2j}$  is the largest among the candidate matches of  $\mathbf{p}_{1i}$  and the largest among the candidate matches of  $\mathbf{p}_{2j}$ .

Suppose that a cubic volumetric image region  $\mathcal{N}(\mathbf{p})$  represents the neighborhood of point  $\mathbf{p}$ , then, we will expect to see many potential matches within their neighborhoods  $\mathcal{N}(\mathbf{p}_{1i})$  and  $\mathcal{N}(\mathbf{p}_{2j})$  if and only if  $(\mathbf{p}_{1i}, \mathbf{p}_{2j})$  is a potential match. In contrast, we will expect to see only a few or even no matches. Let  $(\mathbf{n}_{1k}, \mathbf{n}_{2l})$  be the potential matches within  $\mathcal{N}(\mathbf{p}_{1i})$  and  $\mathcal{N}(\mathbf{p}_{2j})$ , respectively, where  $\mathbf{n}_{1k} \in \mathcal{N}(\mathbf{p}_{1i})$  and  $\mathbf{n}_{2l} \in \mathcal{N}(\mathbf{p}_{2j})$ . More strictly, we define a strength function of candidate matches  $\mathbf{p}_{1i}$  and  $\mathbf{p}_{2j}$  as:

$$SM(\mathbf{p}_{1i}, \mathbf{p}_{2j}) = cs(\mathbf{p}_{1i}, \mathbf{p}_{2j}) + \alpha \sum_{k,l=1}^s \frac{cs(\mathbf{n}_{1k}, \mathbf{n}_{2l}) \cdot \eta(\mathbf{n}_{1k}, \mathbf{n}_{2l})}{1 + diff(\mathbf{p}_{1i}, \mathbf{p}_{2j}; \mathbf{n}_{1k}, \mathbf{n}_{2l})} \quad (13)$$

where  $s$  represents the total number of the potential matches in the neighborhoods  $\mathcal{N}(\mathbf{p}_{1i})$  and  $\mathcal{N}(\mathbf{p}_{2j})$  of the candidate match  $(\mathbf{p}_{1i}, \mathbf{p}_{2j})$ ,  $\alpha$  is a balancing parameter used to balance the weight during iteration, and  $diff(\mathbf{p}_{1i}, \mathbf{p}_{2j}; \mathbf{n}_{1k}, \mathbf{n}_{2l})$  is the relative distance difference given by

$$diff(\mathbf{p}_{1i}, \mathbf{p}_{2j}; \mathbf{n}_{1k}, \mathbf{n}_{2l}) = \frac{d(\mathbf{p}_{1i}, \mathbf{n}_{1k}) - d(\mathbf{p}_{2j}, \mathbf{n}_{2l})}{dist(\mathbf{p}_{1i}, \mathbf{p}_{2j}; \mathbf{n}_{1k}, \mathbf{n}_{2l})} \quad (14)$$

where  $dist(\mathbf{p}_{1i}, \mathbf{p}_{2j}; \mathbf{n}_{1k}, \mathbf{n}_{2l})$  is the average distance between two pairs  $(\mathbf{p}_s, \mathbf{n}_s)$ . Let us define the Euclidean distance between the pair of points  $\mathbf{p}_s$  and  $\mathbf{n}_s$  as

$$d(\mathbf{p}_s, \mathbf{n}_s) = \|\mathbf{p}_s - \mathbf{n}_s\|. \quad (15)$$

We then have

$$dist(\mathbf{p}_{1i}, \mathbf{p}_{2j}; \mathbf{n}_{1k}, \mathbf{n}_{2l}) = \frac{d(\mathbf{p}_{1i}, \mathbf{n}_{1k}) + d(\mathbf{p}_{2j}, \mathbf{n}_{2l})}{2} \quad (16)$$

Generally, with better matched pair  $(\mathbf{n}_{1k}, \mathbf{n}_{2l})$ , we expect more contribution to its center pair  $(\mathbf{p}_{1i}, \mathbf{p}_{2j})$ . Moreover, as is well known, we can measure the similarity between two volumetric image regions by minimising the sum of the square of the residual between the two regions. So, the contribution  $\eta(\mathbf{n}_{1k}, \mathbf{n}_{2l})$  of potentially matched pair  $(\mathbf{n}_{1k}, \mathbf{n}_{2l})$  in equation (13) can be defined by the residual as follows. Let vector  $\mathbf{x}_{\mathbf{n}_{1k}} = (x_{\mathbf{n}_{1k}}, y_{\mathbf{n}_{1k}}, z_{\mathbf{n}_{1k}}) \in \mathcal{N}(\mathbf{n}_{1k})$  represent the coordinate of a voxel in  $\mathcal{N}(\mathbf{n}_{1k})$ , and its corresponding point  $\mathbf{n}_{2l}$  be regarded as its estimation in the deformed volumetric image, then we can use the sum of the square residual of neighborhoods to substitute for the residual of the point  $\mathbf{n}_{1k}$ . Ideally, the residual  $\zeta(\mathbf{n}_{1k}, \mathbf{n}_{2l})$  of  $\mathbf{n}_{1k}$  can be defined as

$$\zeta(\mathbf{n}_{1k}, \mathbf{n}_{2l}) = \sum_{\mathbf{x}_{\mathbf{n}_{1k}} \in \mathcal{N}} |g_{\mathbf{n}_{1k}}(\mathbf{x}_{\mathbf{n}_{1k}}) - g'_{\mathbf{n}_{2l}}(\mathbf{x}_{\mathbf{n}_{1k}})|^2.$$

Considering the rotation transformation between the initial and final volumetric images, we can rewrite the above equation as

$$\zeta(\mathbf{n}_{1k}, \mathbf{n}_{2l}) = \sum_{\mathbf{x}_{\mathbf{n}_{1k}} \in \mathcal{N}} |g_{\mathbf{n}_{1k}}(\mathbf{x}_{\mathbf{n}_{1k}}) - g'_{\mathbf{n}_{2l}}(\mathbf{x}_{\mathbf{n}_{1k}}, \mathcal{R})|^2 \quad (17)$$

where  $g_{\mathbf{n}_{1k}}(\mathbf{x}_{\mathbf{n}_{1k}})$  is the intensity values in the image at position  $\mathbf{x}_{\mathbf{n}_{1k}}$ ,  $g'_{\mathbf{n}_{2l}}(\mathbf{x}_{\mathbf{n}_{1k}}, \mathcal{R})$  is the intensity value of the voxel centered at point  $\mathbf{n}_{2l}$ , and its relative coordinate  $\mathbf{x}_{\mathbf{n}_{2l}} = (x_{\mathbf{n}_{2l}}, y_{\mathbf{n}_{2l}}, z_{\mathbf{n}_{2l}}) \in \mathcal{N}(\mathbf{n}_{2l})$  satisfies

$$[x_{\mathbf{n}_{2l}} \ y_{\mathbf{n}_{2l}} \ z_{\mathbf{n}_{2l}}]^T = \mathcal{R}[x_{\mathbf{n}_{1k}} \ y_{\mathbf{n}_{1k}} \ z_{\mathbf{n}_{1k}}]^T$$

Without losing generality, we define the local contributions of the pair  $(\mathbf{n}_{1k}, \mathbf{n}_{2l})$  via the *Gibbs distribution* in the form

$$\eta(\mathbf{n}_{1k}, \mathbf{n}_{2l}) = \frac{1}{Z(\mathbf{n}_{1k}, \mathbf{n}_{2l})} \cdot \exp^{-\lambda \cdot \zeta(\mathbf{n}_{1k}, \mathbf{n}_{2l})} \quad (18)$$

where the notation  $Z(\mathbf{n}_{1k}, \mathbf{n}_{2l})$  represents the partition function (or normalizing constant) of the pair  $(\mathbf{n}_{1k}, \mathbf{n}_{2l})$ . This is given by

$$Z(\mathbf{n}_{1k}, \mathbf{n}_{2l}) = \sum_{k,l=1}^s \exp^{-\lambda \cdot \zeta(\mathbf{n}_{1k}, \mathbf{n}_{2l})} \quad (19)$$

where  $s$  has the same meaning as equation (13), the attenuation constant  $\lambda = 1/T$  and call  $T$  temperature. Here, we expect to select proper  $\lambda$  so that as  $\lambda$  increases (or  $T$  decreases), the  $\eta(\mathbf{n}_{1k}, \mathbf{n}_{2l})$  of those with large residuals quickly decreases, and ultimately the contributions is mainly from those with the smallest residuals. Thus, in our implementation, we define the attenuation constant  $\lambda$  as

$$\lambda = \frac{1}{T} = \{\zeta(\mathbf{n}_{1k}, \mathbf{n}_{2l}) - \bar{\zeta}\}^2 \quad (20)$$

where  $\bar{\zeta}$  represents the average residuals of potential matches within the neighborhood of the candidate pair  $(\mathbf{p}_{1i}, \mathbf{p}_{2j})$ .

**3) Relaxation labeling:** The relaxation technique was first proposed by Rosenfel et al. [29]. The basic idea is to use iterated local context updates to achieve a globally consistent result [30]. To disambiguate the candidate matches, we define the energy function as the average of the strengths of all candidate matches:

$$\varepsilon = \frac{1}{N} \sum_{i,j=1}^N SM(\mathbf{p}_{1i}, \mathbf{p}_{2j}) \quad (21)$$

where  $N$  is the total number of matched pairs in a potential matches set (PMS) at time  $t$ .

The matches can be disambiguated by maximizing the energy function  $\varepsilon$ , using an iterative procedure. Here, we note that since the PMS varies dynamically, the strength function (13) also varies. Therefore, potential matches can be updated constantly, and the iteration will stop when the energy decreases. The relaxation process can be described as follows in pseudo code.

```

set  $\alpha \leftarrow 0$ 
for( $i = 0$  to total number of points in initial image)
  for( $j = 0$  to total number of candidates of  $\mathbf{p}_{1i}$ 
    in final image)
      if( $\max\{cs(\mathbf{p}_{1i})\} \rightarrow \mathbf{p}_{2j}$  and  $\max\{cs(\mathbf{p}_{2j})\} \rightarrow \mathbf{p}_{1i}$ )
        Add pair( $\mathbf{p}_{1i}, \mathbf{p}_{2j}$ )  $\rightarrow$  PMS;
iteration
{
  for( $n = 0$  to total number of PM pairs)
    Computation the  $SM(\mathbf{p}_{1n}, \mathbf{p}_{2n})$ ;
    Computation the energy function  $\varepsilon_t$ ;
  if( $\varepsilon_t \geq \varepsilon_{t-1}$ )
  {
    PMS  $\leftarrow 0$ ;
    for( $i = 0$  to total number of points in initial image)
      for( $j = 0$  to total number of candidates of  $\mathbf{p}_{1i}$ 
        in final image)
          if( $\max\{SM(\mathbf{p}_{1i})\} \rightarrow \mathbf{p}_{2j}$  and
              $\max\{SM(\mathbf{p}_{2j})\} \rightarrow \mathbf{p}_{1i}$ )
            Add pair( $\mathbf{p}_{1i}, \mathbf{p}_{2j}$ )  $\rightarrow$  PMS;
     $\alpha \leftarrow \alpha + \Delta \alpha$ 
  }
  else
    stop iteration;
}

```

Functions  $\varepsilon_t$  and  $\varepsilon_{t-1}$  are energies at time  $t$  and  $t-1$ , respectively. If  $SM(\mathbf{p}_{1i}, \mathbf{p}_{2j})$  is the largest among the candidate matches for  $\mathbf{p}_{1i}$ , then  $\max\{SM(\mathbf{p}_{1i})\} \rightarrow \mathbf{p}_{2j}$ , and  $\max\{cs(\mathbf{p}_{1i})\} \rightarrow \mathbf{p}_{2j}$  have similar meaning.

Moreover, we should emphasize that the balancing parameter  $\alpha$  increases during the first couple of iterations.

It is worth pointing out the similarities and differences between our algorithm and those reported in references

in [26] [28]. First, the above algorithm is a combination of those proposed by Zhang [26] and Chen [28] and, therefore, they are similar in form. Second, by the potential matches as substitutes for high curvature points in the neighborhood of the candidate match  $(\mathbf{p}_{1,i}, \mathbf{p}_{2,j})$ , the above algorithm can effectively avoid the dissymmetry that may appear in the algorithm proposed in [26]. Third, in addition to differences in distance, our SM function considers the contribution ratio of potential matches of different strength. Normalised *Gibbs distribution* of residual of each pair of potential matches reveals that those pairs that have smaller residual would have larger contribution.

### C. Deformation measurement

Well matched pairs of feature points are used to measure local deformation. Let  $\mathcal{D}$  be the displacement vector of a given point of high curvature in the initial MR volumetric image relative to its corresponding point in the final image,  $\varphi$  represent the angle between the displacement vector and the  $xz$ -plane, and  $\mathbf{x}_1 = (x_1 \ y_1 \ z_1)^T$  and  $\mathbf{x}_2 = (x_2 \ y_2 \ z_2)^T$  represent the coordinate of corresponding points in their respective coordinate systems. Then, we have

$$\mathcal{D} = \|\mathbf{x}_1(\mathcal{R}, \tau) - \mathbf{x}_2\| \quad (22)$$

and

$$\varphi = \arcsin\left(\frac{y_2 - y_1'}{\mathcal{D}}\right) \quad (23)$$

where  $y_1'$  satisfies

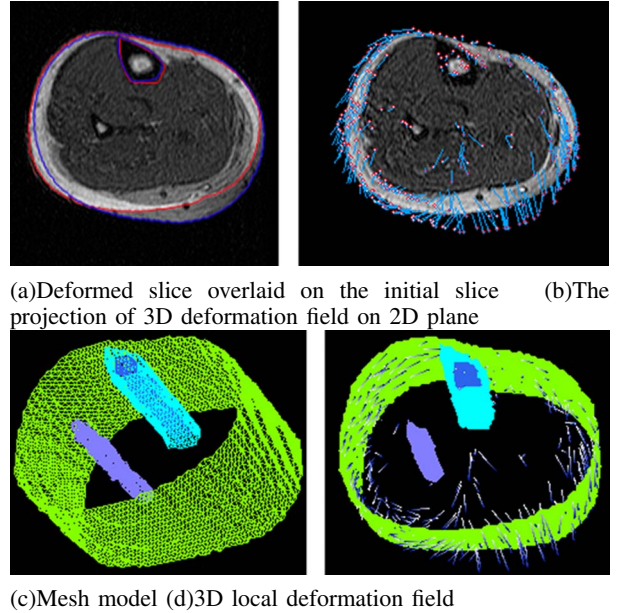
$$[0 \ y_1' \ 0]^T = \mathcal{R}[0 \ y_1 \ 0]^T + \tau. \quad (24)$$

### III. EXPERIMENTS AND RESULTS

To evaluate the proposed approach, we performed a practical experiment using software that we wrote in Visual C++ and ran on Microsoft Windows XP in a Dell PC with a 2.80 GHz Intel® Pentium® D CPU and 1 GB of RAM.

For the experiment, MR volumetric images (Figure 1) of a volunteer's calf were taken under different status and at different times. In both cases, there were 76 slices, FOV was  $20 \times 20$  cm, and the slice gap was 2 mm. In this case, we selected 20 neighbouring slices from each of the initial and final MR volume data sets. For both the initial and deformed images, we performed linear interpolation between two neighboring original slices, which gave discrete volumetric images of size  $256 \times 256 \times 40$  and sufficient resolution along the  $z$ -axis direction.

Figure 3 shows the experiment results. To clarify the extent of deformation, two slices, one from the initial and the other from the deformed series, are superimposed using a uniform coordinate system (Fig.3a). In Figure 3a, the red and blue contours show the edges of the deformed and initial slices, respectively. Figure 3b is their 2D projection of the 3D deformation. Figure 3c shows the 3D mesh model of the final volumetric image, and Figure 3d shows the local deformation



(a)Deformed slice overlaid on the initial slice      (b)The projection of 3D deformation field on 2D plane

(c)Mesh model      (d)3D local deformation field

Fig. 3. Original MR volumetric image

field overlaid on the 3D surface model of the final volumetric image. The arrow with the blue tail and white head indicates the direction and magnitude of the local deformation.

Figure 3 was obtained with a search cube size of  $17 \times 17 \times 7$  voxels and a match cube size of  $9 \times 9 \times 5$  voxels. The total number of reference high curvature points in the initial volumetric images is 500. There were 330 pairs of successful matches, of which 297 (90%) were good. The time cost was 10 seconds.

### IV. CONCLUSION

We proposed a method to measure local deformation in soft biological tissues from MR volumetric by matching pairs of feature points. The core idea is to find points in volumetric images taken before deformation that match points well in the image taken after deformation. After matching points we used a relaxation technique to obtain good matches. Our preliminary experimental results reveal that our approach is effective. Compared with similar types of algorithms, our approach has the following advantages:

- (1) Independent of the initial contours or boundaries.
  - (2) Feature points are automatically extracted from volumetric images.
  - (3) Insensitive to noise.
- In the future, we intend to
- (1) Improve the algorithm so that it is applicable to large deformations.
  - (2) Improve the accuracy of feature point matching.
  - (3) Reduce the number of false matches.

## REFERENCES

- [1] B.J. Matuszewski, Jian-Kun Shen, Lik-Kwan Shark and Moore C., "Estimation of Internal Body Deformations Using an Elastic Registration Technique," *Proceedings of the International Conference on Medical Information Visualisation-BioMedical Visualisation*. Jul. 2006, pp.15-20.
- [2] Jinsoo Cho and Benkeser P.J., "Elastically deformable model-based motion-tracking of left ventricle," *Proceedings of the 26th Annual International Conference of the IEEE EMBS*. Vol. 1, No. 3, Sept. 2004, pp.1925-1928.
- [3] X. Papademetris, Sinusas A.J, Dione D.P, Constable R.T and Duncan J.S, "Estimation of 3-D left ventricular deformation from medical images using biomechanical models," *IEEE Transactions on Medical Imaging*. Vol. 21, No. 7, Jul. 2002, pp.786-800.
- [4] Chenoune Y, Delechelle E, Petit E, Goissen T, Garot J, Rahmouni A, "Segmentation of cardiac cine-MR images and myocardial deformation assessment using level set methods," *Computerized Medical Imaging and Graphics*. Vol. 29, No. 8, Dec. 2005, pp.607-616.
- [5] Kass M., Witkin A. and Terzopoulos D., "Snakes: active contours models," *International Journal of Computer Vision*. Vol. 1, No. 4, Jan. 1987, pp.321-331.
- [6] Jochen Lang, Pai D.K. and Woodham R.J., "Robotic acquisition of deformable models," *IEEE International Conference on Robotics and Automation, 2002. Proceedings. ICRA '02*. Vol. 1, 2002, pp.933- 938.
- [7] Vicent Caselles, Francine Catte, Tomeu Coll, Francoise Dibos, "A geometric model for active contours in image processing," *Numerische Mathematik*. Vol.66, No.1, Dec. 1993, pp.1-31.
- [8] Malladi R., Sethian J.A., Vemuri B.C., "Shape modeling with front propagation: a level set approach," *IEEE Transactions on Pattern Analysis and Machine Intelligence*. Vol.17, No.2, Feb. 1995, pp.158-175.
- [9] Caselles Vicent, "Geometric models for active contours," *International Conference on Image Processing, Proceedings*. Vol. 3, Oct. 1995, pp.19-12.
- [10] Fuzhen Huang, Jianbo Su, "Face Contour Detection Using Geometric Active Contours," *Proceedings of the 4th World Congress on Intelligent Control and Automation. Shanghai*, Vol.3, 2002, pp.2090- 2093.
- [11] E. Zerhouni, D. Parish, W. Rogers, A. Yang, and E. Shapiro, "Human heart: Tagging with MR imaging-A method for noninvasive assessment of myocardial motion," *Radiology*. Vol.169, 1988, pp.59-63.
- [12] Amini A.A., Yasheng Chen, Curwen R.W., Mani, V. and Sun J., "Coupled B-snake grids and constrained thin-plate splines for analysis of 2-D tissue deformations from tagged MRI," *IEEE Transactions on Medical Imaging*. Vol. 17, No. 3, Jun 1998, pp.344-356.
- [13] Jiantao Huang, Dana Abendschein, Victor G. Dávila-Román and Amir A. Amini, "Spatio-Temporal Tracking of Myocardial Deformations with a 4-D B-Spline Model from Tagged MRI," *IEEE TRANSACTIONS ON MEDICAL IMAGING*.Vol.18, No.10, Oct. 1999 , pp. 957-971.
- [14] Y. Wang and A. A. Amini, "Fast computation of tagged MRI motion fields with subspace approximation techniques," *IEEE Workshop on Mathematical Methods in Biomedical Image Analysis, 2000. Proceedings*. June 2000 , pp. 119-126.
- [15] Yasheng Chen, Amini A.A., "A MAP framework for tag line detection in SPAMM data using Markov random fields on the B-spline solid," *IEEE Workshop on Mathematical Methods in Biomedical Image Analysis, 2001. MMBIA.2001*. June 2000 , pp.131-138 .
- [16] M. Betke, H. Hong, and J. P. Ko, "Automatic 3D Registration of Lung Surfaces in Computed Tomography Scans," *Fourth International Conference on Medical Image Computing and Computer-Assisted Intervention MICCAI 2001*. October 2001, pp. 725-733.
- [17] A. Carrillo, J.L. Duerk, J.S. Lewin, D.L. Wilson, "Semiautomatic 3-D image registration as applied to interventional MRI liver cancer treatment," *IEEE Transactions on Medical Imaging*. Vol. 19, No. 3, March 2000 , pp. 175 - 185.
- [18] R.S.Lazebnik, T.L.Lancaster, M.S.Breen, J.S.Lewin, D.L.Wilson, "Volume registration using needle paths and point landmarks for evaluation of interventional MRI treatments," *IEEE Transactions on Medical Imaging*. Vol. 22, No. 5, May 2003, pp. 653 - 660.
- [19] D.Krechel, D.Pedroso, A.von Wangenheim, "Automatic registration of MRI head volumes using an octree anatomical atlas," *12th IEEE Symposium on Computer-Based Medical Systems, 1999. Proceedings*. June 1999, pp. 60 - 65.
- [20] C. Studholme, C. Drapaca, B. Iordanova, V. Cardenas, "Deformation-based mapping of volume change from serial brain MRI in the presence of local tissue contrast change," *IEEE Transactions on Medical Imaging*. Vol. 25, No.5, May 2006, pp. 626 - 639.
- [21] L.G. Nyul, J.K. Udupa, P.K. Saha, "Incorporating a measure of local scale in voxel-based 3-D image registration," *IEEE Transactions on Medical Imaging*. Vol.22, No.2, Feb 2003, pp. 228 - 237.
- [22] T. Eric, B.Jean-Yves, "Elastic registration of MRI scans using fast DCT," *Engineering in Medicine and Biology Society, 2000. Proceedings of the 22nd Annual International Conference of the IEEE*. Vol.4, July 2000 , pp. 2854 - 2856.
- [23] Haili Chui, James Rambo, James Duncan, Robert Schultz, Anand Rangarajan, "Registration of Cortical Anatomical Structures via Robust 3D Point Matching," *Proceedings of the 16th International Conference on Information Processing in Medical Imaging. Visegrad*, Vol.4, July 1999 , pp. 168 - 181.
- [24] Berthold K.P Horn, "Closed Form Solution of Absolute Orientation using Unit Quaternions," *Optical Society of America A: Optics, Image Science, and Vision*. Vol.4, No.4, April 1987 , pp. 629-642.
- [25] Margrit Betke, Harrison Hong, Jane P. Ko, "Automatic 3D Registration of Lung Surfaces in Computed Tomography Scans," *Proceedings of the 4th International Conference on Medical Image Computing and Computer-Assisted Intervention MICCAI 2001. Utrecht*, October 2001, pp. 725-733.
- [26] Zhengyou Zhang, Rachid Deriche, Olivier FAUGERAS, Quang-Tuan LUONG, "A robust technique for matching two uncalibrated images through the recovery of the unknown epipolar geometry," *Special volume on computer vision*. Vol.78, October 1995, pp. 87 - 119.
- [27] ZuXun Zhang, JianQin Zhang, "Correlation score measurement," *Digital Photogrammetry*. Jan 1997, pp. 168 - 169.
- [28] Chen G.Q., "Robust point feature matching in projective space," *Proceedings of the 2001 IEEE Computer Society Conference on Computer Vision and Pattern Recognition, 2001. CVPR 2001. Hawaii USA*, Vol.1, 2001, pp. 717 - 722.
- [29] A. Rosenfeld, R. A. Hummel and S. W. Zucker, "Scene Labeling by Relaxation Operations," *IEEE Transactions on Systems, Man, and Cybernetics*. 1976, pp. 420-433.
- [30] Yefeng Zheng, Doermann, D., "Scene Labeling by Relaxation Operations," *IEEE TRANSACTIONS ON PATTERN ANALYSIS AND MACHINE INTELLIGENCE*. Vol. 28, No. 4, April 2006, pp. 643-649.
- [31] C. Harris and M.J. Stephens, "A combined corner and edge detector," *Proceedings of The Fourth Alvey Vision Conference*. 1988, pp. 147-151.